Computer simulation study on the swelling of a polyelectrolyte gel by a Stockmayer solvent

Z.-Y. Lu* and R. Hentschke†
FB Physik and Institut für Materialwissenschaften, Bergische Universität, D-42097 Wuppertal, Germany
(Received 13 February 2003; published 30 June 2003)

The swelling of a model polyelectrolyte gel is studied via three-dimensional molecular dynamics simulations, taking into account the counterions and the solvent explicitly. Each network bead carries a charge q^*. The counterion charge is $-q^*$, and thus the total system is neutral. The solvent is modeled via a Stockmayer fluid, i.e., each solvent particle is a point dipole plus a Lennard-Jones interaction center. A ''two-box–particle transfer'' simulation method is applied to calculate the swelling ratio of the network as well as the counterion mobility. The swelling of the network shows a broad maximum as a function of q^* at $T_r^*=T^*/T_c^*=1.05$ and $P_r^*=P^*/P_c^*=1.0$. Here, T_c^* and P_c^* are the critical temperature and the critical pressure of the pure Stockmayer solvent, respectively, with dipole moments given by $\mu^{*2}=1.0$, 2.0, 3.0, and 4.0. The residence time of the counterions is calculated, showing a strong coupling to the charged network beads (condensation) as q^* increases. Additional simulations at three different charge strengths (i.e., $q^*=0.5$, 3.5, and 8.6) illustrate the complicated swelling behavior of the network under supercritical and subcritical conditions.

DOI: 10.1103/PhysRevE.67.061807 PACS number(s): 61.25.Hq, 05.10.−a, 82.70.Gg, 82.60.Lf

I. INTRODUCTION

Polyelectrolytes, charged polymers which can dissociate ions in polar solvent, have many industrial applications (e.g., diapers) and play an important role in the biological sciences (e.g., DNA and proteins) [1–3]. Theoretical prediction of polyelectrolyte behavior is more difficult than in the case of neutral polymers. Due to the long-range nature of electrostatic interactions and the existence of counterions, polyelectrolyte systems possess several different length and time scales. Therefore, analytic theory or scaling auguments become very complicated [4]. Computer simulations, even though these too are more difficult in the case of polyelectrolytes, can serve as an alternative tool to investigate conformational and dynamical properties on a nanoscopic level [4–6].

Polyelectrolytes can form networks which swell or shrink in response to the change of thermodynamic conditions. Compared to the neutral network, there are new factors, such as network charge density and the polarity of the solvent, which are essential to the swelling. Because polyelectrolyte networks are so complicated, detailed studies on the microscopic level are scarce. The swelling of a two-dimensional polyelectrolyte gel was simulated by Aalberts [7]. His model, which yields a first-order phase transition, is highly simplified, and the ionic groups are not simulated explicitly but a counterion pressure is introduced instead to mimic the osmotic pressure due to the counterions. However, three-dimensional simulation studies including the ionizable groups in the network, explicit counterions, and explicit solvent are needed, because this kind of detail is necessary to generate a realistic gel behavior [8]. Schneider and Linse simulated the swelling of a three-dimensional defect-free polyelectrolyte gel, with explicit counterion but without explicit solvent particles, using Monte Carlo [9]. Their model polyelectrolyte gel displays a large swelling capacity compared to the corresponding uncharged polymer network.

To the best of our knowledge this work is a first attempt to study the swelling behavior of a model polyelectrolyte gel, with explicit counterions and explicit solvent particles, using a three-dimensional molecular dynamics simulation method. Each network bead carries a partial charge q^* and the corresponding dissociable counterion charge $-q^*$. The total system is neutral. The explicitly considered solvent particles interact via a Stockmayer potential [10]. The simulated swelling ratio of the network exhibits a broad peak as a function of q^* at $T_r^*=T^*/T_c^*=1.05$ and $P_r^*=P^*/P_c^*=1.0$. T_c^* and P_c^* are the critical temperature and the critical pressure of the Stockmayer solvent, respectively, with the dipole moments $\mu^*=1.0$, $\sqrt{2.0}$, $\sqrt{3.0}$, and 2.0. We show that as q^* increases, there is a progressive condensation of counterions. Such a condensation will reduce the electrostatic repulsion between network charges, which initially tends to increase the swelling ratio, so that the configuration entropy of the network strands may finally reduce the swelling. The residence time of the counterions in the vicinity of the network beads is calculated, showing that the counterions strongly couple to the polyelectrolyte network after condensation takes place. Additional simulations for three different charge strengths ($q^*=0.5$, 3.5, and 8.6) show a complicated swelling behavior at both subcritical and supercritical temperatures for $\mu^{*2}=1.0$.

II. SIMULATION METHOD AND MODEL CONSTRUCTION

In this study, we apply our recently developed ''two-box–particle transfer'' molecular dynamics simulation method. This method, which is discussed in detail in Refs. [11–13], is suitable for studying the swelling behavior of model polymer networks under varying thermodynamic conditions including solvent dynamics. In brief, two simulation boxes are coupled together; one is the network box containing counterions and

*Permanent address: Institute of Theoretical Chemistry, Jilin University, 130023 Changchun, China.
†Author to whom correspondence should be addressed.

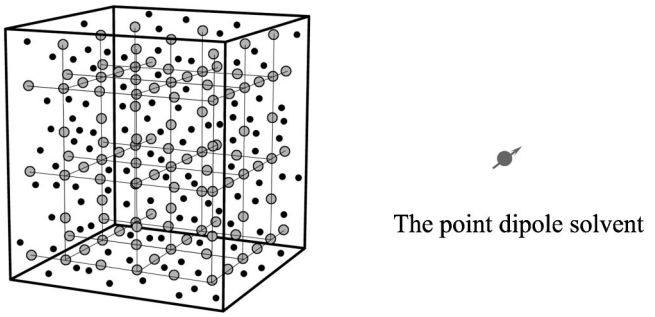

FIG. 1. A sketch of the polyelectrolyte network (gray) with counterions (black) and the point dipole solvent used in the simulations.

solvent particles, whereas the other contains pure solvent. These two boxes can exchange solvent particles during the simulation. The exchange is controlled by decreasing the solvent chemical potential difference between the boxes at the same average temperature and pressure.

In this study, we model the solvent as a Stockmayer fluid, i.e., the potential energy between two solvent particles is

$$U_{\mu}(\boldsymbol{r}_{ij},\boldsymbol{\mu}_i,\boldsymbol{\mu}_j)=4\varepsilon\left[\left(\frac{\sigma}{r_{ij}}\right)^{12}-\left(\frac{\sigma}{r_{ij}}\right)^{6}\right]+\frac{1}{4\pi\epsilon_0 r_{ij}^3}\times\left[\boldsymbol{\mu}_i\cdot\boldsymbol{\mu}_j-\frac{3(\boldsymbol{r}_{ij}\cdot\boldsymbol{\mu}_i)(\boldsymbol{r}_{ij}\cdot\boldsymbol{\mu}_j)}{r_{ij}^2}\right], \quad (1)$$

where $r_{ij}=|\boldsymbol{r}_i-\boldsymbol{r}_j|$ is the distance between two interaction centers, ε and σ are Lennard-Jones parameters, which are equal to one in the following, $\boldsymbol{\mu}_i$ is the point-dipole moment vector of particle i, and ϵ_0 is the permittivity of vacuum.

The polyelectrolyte network used in this work, a sketch including the counterions and the Stockmayer solvent is shown in Fig. 1, possesses the same cubic symmetry as used before in the case of ''neutral'' network (cf., Refs. [13,14]). In this coarse-grained model, every second interaction center along the chain is a crosslink. A partial charge q^* is assigned to each network bead. Correspondingly, $-q^*$ is assigned to every counterion. Overall, the system is neutral. The asterisk means that q is scaled via $q^*=q/\sqrt{4\pi\epsilon_0\sigma\varepsilon}$. The interactions between these charged particles (U_c) are of Lennard-Jones type (U_{LJ}) with an added Coulomb part (U_q):

$$U_c=U_{LJ}+U_q, \quad (2)$$

$$U_{LJ}(r_{ij})=4\varepsilon\left[\left(\frac{\sigma}{r_{ij}}\right)^{12}-\left(\frac{\sigma}{r_{ij}}\right)^{6}\right], \quad (3)$$

$$U_q(r_{ij})=\frac{q_i q_j}{4\pi\epsilon_0 r_{ij}}. \quad (4)$$

For the network beads and the counterions, we also use $\varepsilon=\sigma=1$. Note that, in the network box, there are also interactions between the solvent and the charged particles in addition to solvent-solvent interactions. The interaction between solvent and charged particles is described also by Eq. (1), where the dipole-dipole term is replaced by the charge-dipole term given by

$$U_{q\mu}(\boldsymbol{r}_{ij},q_i,\boldsymbol{\mu}_j)=\frac{q_i(\boldsymbol{r}_{ij}\cdot\boldsymbol{\mu}_j)}{4\pi\epsilon_0 r_{ij}^3}. \quad (5)$$

Periodic boundary conditions are applied to both simulation boxes separately. In this work, the long-range electrostatic interactions (including charge-charge, charge-dipole, and dipole-dipole interactions) are calculated via the Ewald summation [15–17]. An elegant description of the Ewald summation, including the extension to atomic dipoles and higher-order multipoles, is given by Smith [18]. A discussion of how to treat polarizability can be found in Ref. [19]. In its basic version, the computational effort of this method increases proportional to N^2, where N is the number of interaction centers. However, choosing optimized parameters will result in an order $N^{3/2}$ algorithm [16,20]. An alternative algorithm, which is called particle mesh Ewald (PME) summation, was developed by Darden *et al.* [21]. This very efficient $N\ln(N)$ algorithm may be further revised to calculate the gradients analytically, which significantly improves the accuracy [22]. An extension, including fixed and induced dipolar interactions, was worked out by Toukmaji *et al.* [23]. The basic idea of PME is to split the electrostatic potential into two parts. The first part converges fast enough and can be calculated via the normal cutoff method in the real space. The second part is calculated in the reciprocal space via the fast Fourier transform on a mesh to speed up the calculation. In our case, the electrostatic interaction energy calculated in the real space, U_{dir}, is given by

$$U_{dir}=\frac{1}{2}\sum_{i,j=1}^{N}(q_i+\boldsymbol{\mu}_i\cdot\boldsymbol{\nabla}_i)\times(q_j-\boldsymbol{\mu}_j\cdot\boldsymbol{\nabla}_j)\frac{\mathrm{erfc}(\alpha r_{ij})}{r_{ij}}, \quad (6)$$

where α is the Ewald parameter and $\mathrm{erfc}(x)$ is the complementary error function. The reciprocal energy U_{rec} is given by

$$U_{rec}=\frac{1}{2\pi V}\sum_{\mathbf{m}\neq 0}\frac{\exp(-\pi^2\alpha^2\mathbf{m}^2)}{\mathbf{m}^2}S(\mathbf{m})S(-\mathbf{m}), \quad (7)$$

where the structure factor $S(\mathbf{m})$ can be written as

$$S(\mathbf{m})=\sum_{j=1}^{N}(q_j+2\pi i\boldsymbol{\mu}_j\cdot\boldsymbol{\nabla}_j)\exp(2\pi i\mathbf{m}\cdot\boldsymbol{r}_j). \quad (8)$$

Here, V is the volume of a simulation box and $\mathbf{m}$ is a reciprocal lattice vector. In addition, there is a self-energy U_{self}, due to the interactions of charges and dipoles with themselves, which must be removed. This self-term is given by

$$U_{self}=-\frac{\alpha}{\sqrt{\pi}}\sum_{j}^{N}\left(q_j^2+\frac{2\alpha^2}{3}|\boldsymbol{\mu}_j|^2\right). \quad (9)$$

In this work, we model short-range interactions via Lennard-Jones potentials using a cutoff of 2.9, and long-range interactions, $U_e = U_{dir} + U_{rec} + U_{self}$, are calculated via the smooth PME method [23].

In addition to the equations of translational motion, which are the same as in Ref. [11], we also need to consider the equations of rotational motion for the point dipoles. Defining $\boldsymbol{\mu}_j = \mu \boldsymbol{s}_j$ with $|\boldsymbol{s}_j| = 1$ and $\boldsymbol{G}_j = -\nabla_{\boldsymbol{s}_j} U_e$, we have [15,24]

$$\dot{\boldsymbol{s}}_j = \boldsymbol{u}_j \tag{10}$$

and

$$\dot{\boldsymbol{u}}_j = \boldsymbol{G}_j^{\perp}/I_j + \lambda_j \boldsymbol{s}_j, \tag{11}$$

where $\boldsymbol{u}_j$ is the time derivative of $\boldsymbol{s}_j$, $\boldsymbol{G}_j^{\perp} = \boldsymbol{G}_j - (\boldsymbol{G}_j \cdot \boldsymbol{s}_j)\boldsymbol{s}_j$, I_j is the moment of inertia of point dipole j, and λ_j is used to constrain the length of the dipole vector to a constant value. The translational and rotational equations of motion are numerically solved using a leap-frog algorithm [15]. Constant pressure and temperature are maintained via the Berendsen barostat and thermostat [25] applied to the translational degrees of freedom. Note that, because the translation and the rotation of a dipole are coupled, their respective equilibrium temperatures are the same.

During the simulation, it is important to calculate the solvent chemical potential in each box accurately. If the density of the system is not too high, Widom's test particle method [26] is a good choice. In our *N-P-T* (constant total number of particles, constant pressure, and temperature) simulations, the solvent chemical potential is calculated via Shing and Chung's version of the test particle method including the fluctuation of volume [27]. However, note that Berendsen's method does not produce *N-P-T*-ensemble average. Nevertheless, the error is $O(1/N)$ and should not affect our results significantly.

At the beginning of each simulation run, the network box contains 108 nontransferable network beads, an equal number of counterions, and 192 solvent particles. The pure solvent box contains 700 solvent particles. The integration time step is $\Delta t = 3.80 \times 10^{-4}$ in Lennard-Jones units. To relax the unfavorable network structure, we execute 10^5 time steps under *N-V-T* conditions without allowing solvent transfer. Subsequently the *NPT* simulation is started, allowing solvent exchange. Typical simulation runs range from 1.0×10^6 to 2.0×10^6 time steps. The solvent chemical potential is calculated continuously using Widom test particle method. Each chemical potential value is based on 2×10^3 simulation time steps; for every configuration, 20 test solvent particles are generated at random positions in each of the boxes (with randomly orientated dipole vectors) [11]. A solvent particle will be transferred depending on the difference of the solvent chemical potential between the two simulation boxes.

III. RESULTS AND DISCUSSION

Before we discuss the results pertaining to the swelling behavior of the network, we want to list a number of checks run to test the algorithm. First, we calculate the Madelung constant M of an fcc type lattice and compare our result to the value in Ref. [28]. Our calculation is based on a crystal cell containing 256 ion pairs using periodic boundary conditions. Figure 2 shows the dependence of M on the Ewald parameter α. Note that, in a wide region of α values ($\alpha = 0.35$–0.65 Å^{-1}), the calculated Madelung constant, i.e., 1.747565, coincides with the literature value. The lowest acceptable α value, i.e., $\alpha = 0.35$ Å^{-1}, is used in the following in order to minimize the computational effort.

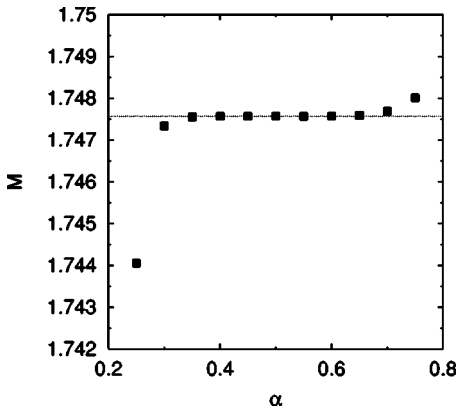

FIG. 2. The dependence of the Madelung constant M on the Ewald parameter α. Symbols: this work; dotted line: literature value taken from Ref. [28].

We also calculate the excess chemical potential for a pure Stockmayer fluid and compare our results with the published data. In this case, 108 point-dipole particles (with $\mu^{*2} = 1.0$) are distributed in a simulation box kept at constant density $\rho^* = 0.8$ and temperature $T^* = 1.35$. The excess chemical potential is calculated via Widom's method during the simulation. The entire run consists of 3.0×10^5 time steps. At each time step, 20 test particles are generated at random positions and with random orientations. In this paper, to distinguish the chemical potential from the notation used for the dipole moment, c^* denotes the chemical potential, and c_{ex}^* denotes the excess chemical potential. Figure 3 shows the simulated excess chemical potential c_{ex}^* based on the cumulative average of $\exp[\beta c_{ex}^*(t)]$ vs time t. Here, $c_{ex}^*(t)$

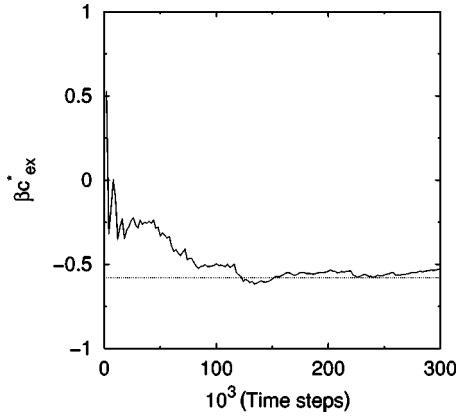

FIG. 3. The cumulative average of the simulated excess chemical potential at $T^* = 1.35$, and $\rho^* = 0.8$. The dotted line corresponds to the literature value obtained from Ref. [29].

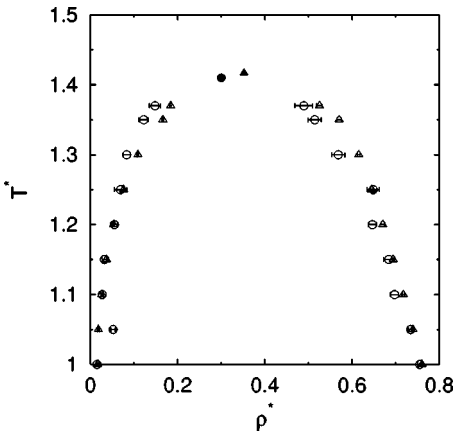

FIG. 4. The gas-liquid coexistence curve for a pure Stockmayer fluid with $\mu^{*2}=1.0$. Triangles: this work; squares: Smit *et al.* [30]. Solid symbols denote the respective critical points.

denotes the instantaneous value, and $\beta=1/k_BT^*$. We obtain $\beta c_{ex}^*=-0.54$ in comparison to $\beta c_{ex}^*=-0.58$ obtained from a Monte Carlo simulation [29].

Using the two-box–particle transfer method, we also calculate the gas-liquid phase coexistence curve for a pure Stockmayer fluid. In this simulation, 620 point dipoles ($\mu^{*2}=1.0$) are used, and the cutoff r_c^* is 2.9. The resulting coexistence curve is shown in Fig. 4. The values used for comparison are taken from Ref. [30]. By fitting the coexistence curve to a power law $\rho_l-\rho_g=B(T-T_c)^{0.32}$ [16], where 0.32 is the approximate order parameter exponent for three-dimensional Ising systems and B is an adjustable parameter, we obtain the critical temperature and density ($T_c^*=1.42, \rho_c^*=0.35$). For comparison, $T_c^*=1.41$ and $\rho_c^*=0.30$ are the values obtained in Ref. [30]. Although there is a small systematic deviation between our coexistence curve and the one in Ref. [30] (which may arise due to the different system sizes and different cutoffs in the two simulations), the resulting critical temperatures are in good accord. Therefore, in the following simulations, we use the published critical temperatures from Ref. [30] for $\mu^{*2}=1.0$, 2.0 and from Ref. [31] for $\mu^{*2}=3.0$, 4.0 to scale our temperatures to avoid time-consuming coexistence curve calculations.

Now we consider the full system, i.e., one box containing the network plus solvent and the second box containing solvent only. In Fig. 5, we show a typical approach to equilibrium. At $T_r^*=0.96$ and $P_r^*=2.16$, the chemical potentials of the dipole solvent with $\mu^{*2}=1.0$ are calculated via Widom's test particle method in the network and the solvent box. Figure 5(a) shows that the exchange of solvent particles leads to the same solvent chemical potential in both boxes. Note that βc^* in the network box fluctuates more strongly compared to the solvent box. Figure 5(b) shows how the solvent number densities ρ^* evolving, analogous to the chemical potentials.

The network swelling ratio is defined as $Q=V/V_0$, where V is the equilibrium volume of the swollen network and V_0 is the equilibrium volume of the ''dry'' network under the same thermodynamic conditions. Here, the ''dry'' network contains the polyelectrolyte including the counterions. It is interesting to see how the charge strength of the network changes its swelling behavior. Thus, close to the solvent critical point ($T_r^*=1.05$ and $P_r^*=1.0$), we simulate Q vs q^* for different dipole strengths, i.e., $\mu^{*2}=1.0$, 2.0, 3.0, and 4.0. The results are shown in Fig. 6. With the increasing charge strength, Q shows a broad maximum. This maximum decreases and slightly broadens with increasing solvent dipole strength, which is due to an increased attendant screening of the charges resulting from the larger solvent dipole moment. In the cases of polyelectrolyte chains, Winkler *et al.* [6] show that by increasing the parameter $\lambda=q_iq_j/4\pi\varepsilon\epsilon\sigma$, which is related to the Bjerrum length, the radius of gyration of the chains also exhibits a maximum. The authors attribute this to counterion condensation according to the interpretation in Ref. [4]. Our simulation results show that polyelectrolyte networks behave similarly, i.e., initially, the increase of q^* leads to an increasing repulsion between charges fixed on the network and thus to an increasing Q. When the counterions condense against the polymer network, the repulsion is diminished by screening, and the stretching of the network segments is entropically reduced. To verify this, we calculate the radial pair distribution function $g^{+-}(r)$ between network charges and counterions for $\mu^{*2}=1.0$. The maximum of the nearest neighbor peak $g_{max}^{+-}(r)$ and the corresponding peak position r_{max} vs the network charge strength q^* are shown in Fig. 7(a). At low q^*, both $g_{max}^{+-}(r)$ and r_{max} vary nonmonotonically. However, the changes are quite small. With

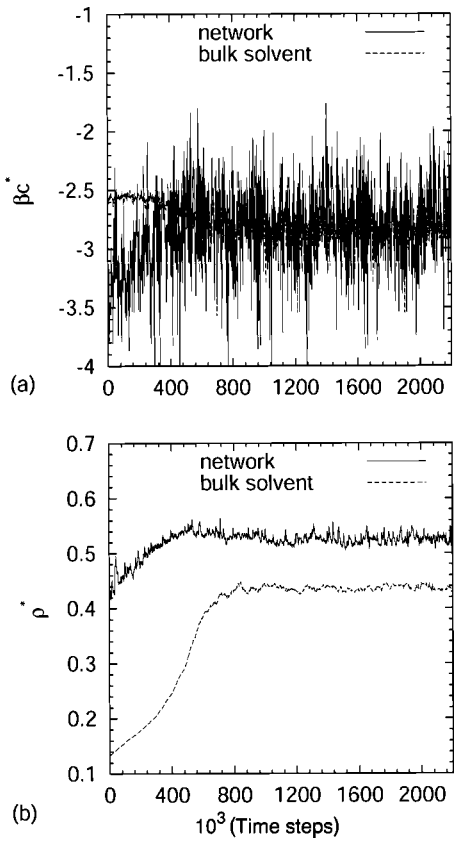

FIG. 5. A typical approach to equilibrium shown at $T_r^*=0.96$ and $P_r^*=2.16$. Solid line: network box; dashed line: bulk dipole solvent.

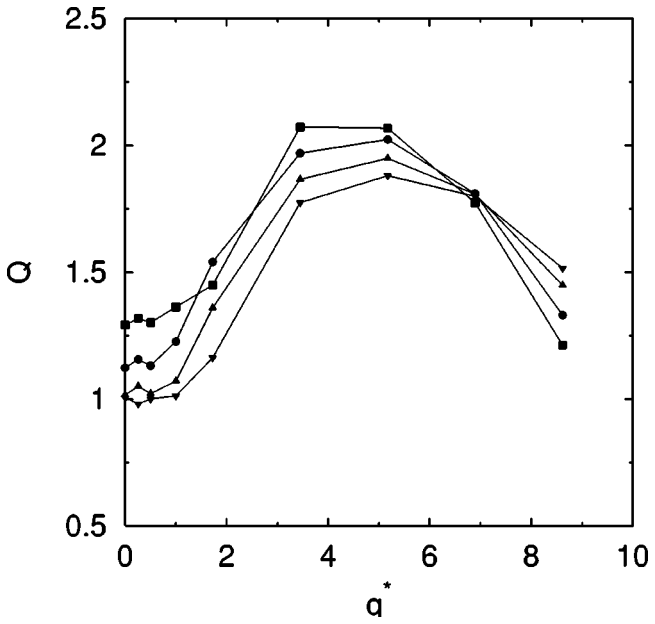

FIG. 6. The swelling ratio a of the network vs charge strength q^* at $T_r^*=1.05$ and $P_r^*=1.0$. The different curves are for different dipole strengths. Squares: $\mu^{*2}=1.0$; circles: $\mu^{*2}=2.0$; up triangles: $\mu^{*2}=3.0$; down triangles: $\mu^{*2}=4.0$.

increasing charge strength, $g_{max}^{+-}(r)$ increases monotonically, and the corresponding r_{max} decreases from roughly 1.1σ to 1.0σ. Because $g_{max}^{+-}(r)$ describes the extent of ion-counterion pair formation and the corresponding r_{max} is the average distance of the nearest counterions from the network beads, we find from Fig. 7(a) that the counterions begin to condense on the charged network at an intermediate q^* value, and this condensation becomes stronger with increasing charge strength. Figure 7(b) shows the number of counterions n within a distance 1.1σ of the network beads, which also increases with increasing q^* (at large charge strength). Thus, Fig. 7 supports our above interpretation.

Another measure of counterion condensation is their mobility. The dynamics of the counterions near the network charges is reflected by their residence time, which was first introduced by Impey *et al.* [32]. First, we define a simple function $P(t,t_0)$, which is one if the counterion resides within a distance 1.1σ of the network bead at both t_0 and t_0+t. Otherwise, it is zero. The average number of counterions residing in the vicinity of a network bead at t_α and at $t_\alpha+t$, $n(t)$ is

$$n(t)=\frac{1}{N_t-t}\frac{1}{N_{network}}\sum_{\alpha=1}^{N_t-t}\sum_{i=1}^{N_{network}}\sum_{j=1}^{N_{counterion}}P_{ij}(t,t_\alpha), \tag{12}$$

where N_t is the total number of time steps, $N_{network}$ is the number of network beads in the system, and $N_{counterion}$ is the number of counterions. $n(t)$ decays exponentially, i.e., $n(t)=n(0)\exp(-t/\tau)$, where τ is the residence time. Figure 8 shows the calculated τ for the counterions vs q^* in the case of $\mu^{*2}=1.0$ at $T_r^*=1.05$ and $P_r^*=1.0$. Note that τ

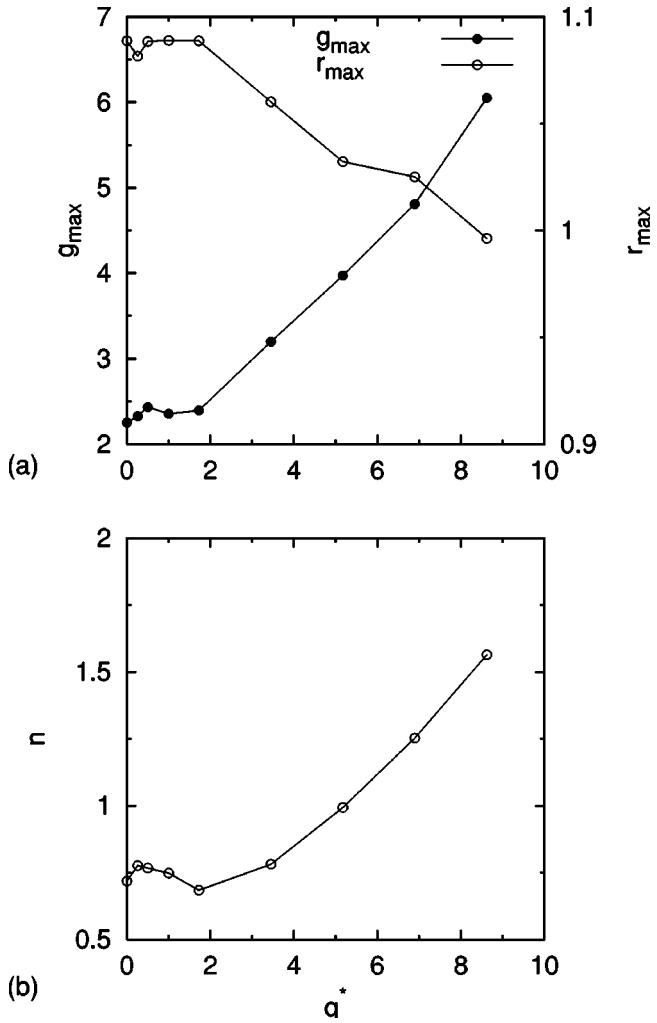

FIG. 7. (a) The height of the nearest neighbor peak of the radial pair distribution function $g_{max}^{+-}(r)$ and the corresponding radial peak position, r_{max} vs charge strength q^*. (b) The average number of counterions within a distance 1.1σ of the central network bead n vs charge strength q^*.

exhibits an overall increase with increasing q^*, which again indicates that the counterions strongly couple to the charged network beads.

In the following, we compare the swelling behavior of our polyelectrolyte network under supercritical and subcritical conditions of the dipole solvent with $\mu^{*2}=1.0$. The swelling ratios Q for networks with three different charge strengths ($q^*=0.5$, 3.5, and 8.6) are shown in Fig. 9 for $T_r^*=0.96$ and $T_r^*=1.91$. At $T_r^*=1.91$, all networks swell monotonically with the increasing pressure. At low pressure, the network with high charge strength swells more strongly than that with low charge strength, whereas at high pressure the network with high charge strength ($q^*=8.6$) swells less than that with smaller charge strength ($q^*=3.5$). At $T_r^*=0.96$, the network with $q^*=0.5$ shows a broad peak in the swelling curve. For the larger charge strengths, the network swells monotonically. Note that for $q^*=3.5$, the swelling is much more pronounced than for $q^*=0.5$ and 8.6. Thus, at $T_r^*=0.96$, by increasing the charge strength, the swelling ratio

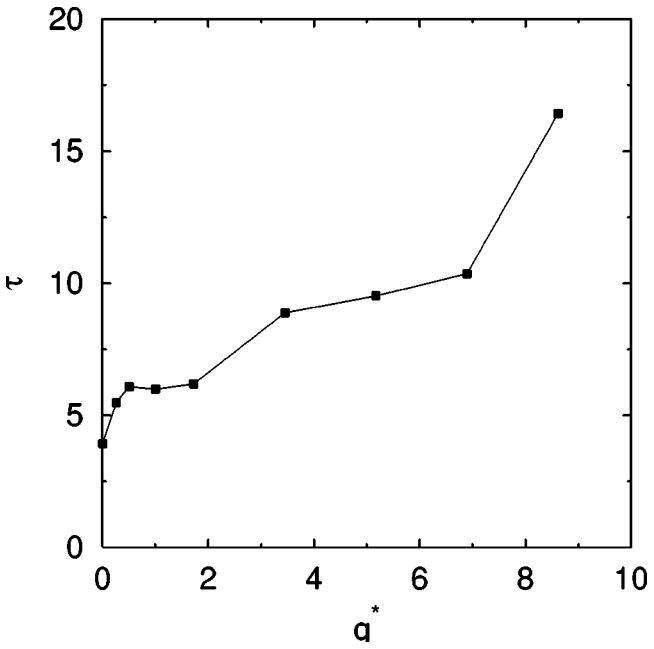

FIG. 8. The reduced residence time τ, expressed in Lennard-Jones units, vs charge strength q^*.

exhibits a peak at around $q^*=3.5$, which is similar to the results obtained at $T_r^*=1.05$ (cf. Fig. 6).

Figure 10 shows a comparison between the swelling behavior of the polyelectrolyte network and the uncharged Lennard-Jones network under the same thermodynamic conditions. The data for the uncharged Lennard-Jones network are taken from Ref. [11]. For both temperatures studied here ($T^*=2.70$ and $T^*=1.35$), the network with intermediate charge strength i.e., $q^*=3.5$ (which is near to the peak in

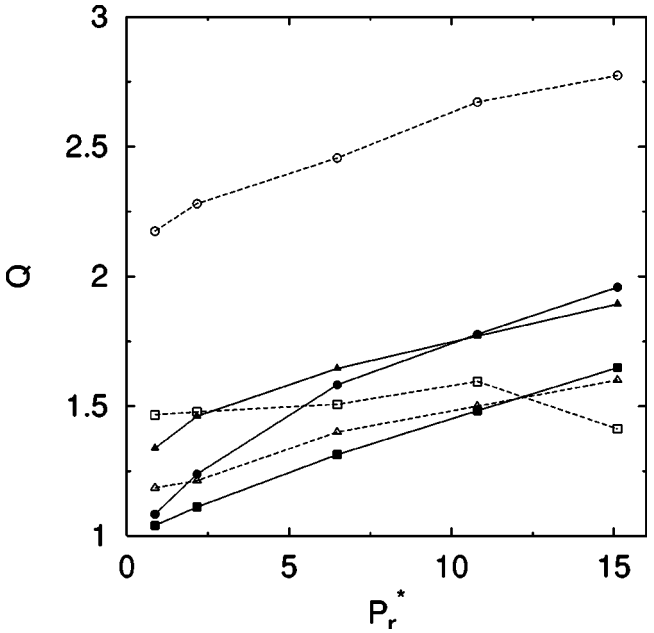

FIG. 9. Swelling ratio Q vs P_r^* obtained under subcritical and supercritical conditions. Solid symbols: $T_r^*=1.91$; hollow symbols: $T_r^*=0.96$. Squares: $q^*=0.5$; circles: $q^*=3.5$; triangles: $q^*=8.6$.

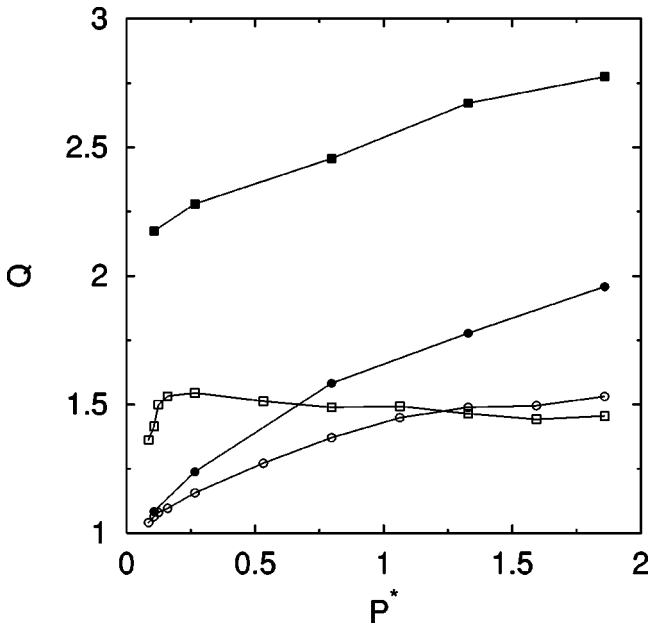

FIG. 10. Comparison of the swelling behavior between the polyelectrolyte network and the pure Lennard-Jones network. Solid squares: $q^*=3.5$, $T^*=1.35$; solid circles: $q^*=3.5$, $T^*=2.70$; hollow squares: pure LJ-system, $T^*=1.35$; hollow circles: pure Lennard-Jones (LJ), $T^*=2.70$.

Fig. 6), swells monotonically with increasing pressure. For $T^*=2.70$, the pure Lennard-Jones network swells monotonically, whereas for $T^*=1.35$ it exhibits a peak in the swelling curve with increasing pressure. The overall swelling ratios of the polyelectrolyte network are always larger than those of the neutral polymer network, which coincides with the result in Ref. [9]. Note that, in the simulations of the polyelectrolyte network, we use a dipole solvent with $\mu^{*2}=1.0$. Therefore, $T^*=1.35$ corresponds to $T_r^*=0.96$, and $T^*=2.70$ corresponds to $T_r^*=1.91$. By combining Figs. 9 and 10, we find that the network with the low charge strength, $q^*=0.5$, has a similar swelling behavior as the neutral Lennard-Jones network. Thus, a weak charging does not significantly change our networks' swelling behavior. However, the network with the high charge strength, i.e., $q^*=8.6$, at which counterion condensation and the attendant screening occur, shows a similar swelling behavior as the network with $q^*=3.5$ but with diminished swelling ratios.

IV. CONCLUSION

In a series of previous papers [11–13], we have investigated the swelling of uncharged model polymer networks using both the computer simulations and the lattice theory. In this work, we have extended our simulation methodology to include polyelectrolyte networks in contact with an explicit polar solvent. The interactions, Lennard-Jones plus monopole-monopole, monopole-dipole, and dipole-dipole interactions, were kept simple to study the main effects due to changing the charge strength q^* of the polyelectrolyte as well as the dipole strength of the Stockmayer solvent. The molecular dynamics simulations, which were carried out at

fixed temperature and pressure, show a maximum of the swelling ratio as a function of q^*. This effect, which results due to a competition between electrostatic repulsion and the network conformational entropy, is also known from the study of ordinary polyelectrolytes. The effect is reduced if the dipole moment of the Stockmayer fluid is increased. In addition, we have calculated the residence time of the counterions, which shows that the counterions are coupled strongly to the charged network bead after condensation. Finally, we have simulated the swelling ratio as a function of pressure at two temperatures slightly below and above the critical solvent temperature. This work shows that our simulation technique is well suited to study the model polyelectrolyte network even including explicit solvent.

ACKNOWLEDGMENT

We are grateful for valuable discussions with Dr. Christian Holm.

[1] *Advances in Polymer Sciences*, edited by K. Dusek (Springer-Verlag, New York, 1993), Vol. 109.
[2] *Advances in Polymer Sciences*, edited by K. Dusek (Springer-Verlag, New York, 1993), Vol. 110.
[3] F. L. Buchholz and N. A. Peppas, in *ACS Symposium Series*, edited by M. J. Comstock (American Chemical Society, Washington, DC, 1994), Vol. 573.
[4] M.J. Stevens and K. Kremer, J. Chem. Phys. **103**, 1669 (1995).
[5] U. Micka, C. Holm, and K. Kremer, Langmuir **15**, 4033 (1999).
[6] R.G. Winkler, M. Gold, and P. Reineker, Phys. Rev. Lett. **80**, 3731 (1998).
[7] D.P. Aalberts, J. Chem. Phys. **104**, 4309 (1996).
[8] F.A. Escobedo and J.J. de Pablo, Phys. Rep. **318**, 85 (1999).
[9] S. Schneider and P. Linse, Eur. Phys. J. E **8**, 457 (2002).
[10] W.H. Stockmayer, J. Chem. Phys. **9**, 398 (1941).
[11] Z.-Y. Lu and R. Hentschke, Phys. Rev. E **63**, 051801 (2001).
[12] Z.-Y. Lu and R. Hentschke, Phys. Rev. E **65**, 041807 (2002).
[13] Z.-Y. Lu and R. Hentschke, Phys. Rev. E **66**, 041803 (2002).
[14] E.M. Aydt and R. Hentschke, J. Chem. Phys. **112**, 5480 (2000).
[15] M. P. Allen and D. J. Tildesley, *Computer Simulation of Liquids* (Oxford University Press, Oxford, 1989).
[16] D. Frenkel and B. Smit, *Understanding Molecular Simulation: From Algorithms to Applications* (Academic, New York, 1996).
[17] D. C. Rapaport, *The Art of Molecular Dynamics Simulation* (Cambridge University Press, Cambridge, 1997).
[18] W. Smith, CCP5 Info. Quart. **4**, 13 (1982).
[19] T.M. Nymand and P. Linse, J. Chem. Phys. **112**, 6152 (2000).
[20] N. Karasawa and W.A. Goddard, J. Phys. Chem. **93**, 7320 (1989).
[21] T. Darden, D. York, and L. Pedersen, J. Chem. Phys. **98**, 10 089 (1993).
[22] U. Essmann, L. Perera, M.L. Berkowitz, T. Darden, H. Lee, and L.G. Pedersen, J. Chem. Phys. **103**, 8577 (1995).
[23] A. Toukmaji, C. Sagui, J. Board, and T. Darden, J. Chem. Phys. **113**, 10 913 (2000).
[24] K. Singer, A. Taylor, and J.V.L. Singer, Mol. Phys. **33**, 1757 (1977).
[25] H.J.C. Berendsen, J.P.M. Postma, W.F. van Gunsteren, A. DiNola, and J.R. Haak, J. Chem. Phys. **81**, 3684 (1984).
[26] B. Widom, J. Chem. Phys. **39**, 2808 (1963).
[27] K.S. Shing and S.T. Chung, J. Phys. Chem. **91**, 1674 (1987).
[28] C. Kittel, *Introduction to Solid State Physics* (Wiley, New York, 1996).
[29] K.K. Han, J.H. Cushman, and D.J. Diestler, J. Chem. Phys. **96**, 7867 (1992).
[30] B. Smit, C.P. Williams, E.M. Hendriks, and S.W. de Leeuw, Mol. Phys. **68**, 765 (1989).
[31] M.E. van Leeuwen, B. Smit, and E.M. Hendriks, Mol. Phys. **78**, 271 (1993).
[32] R.W. Impey, P.A. Madden, and I.R. McDonald, J. Phys. Chem. **87**, 5071 (1983).